International Journal of Applied Earth Observations and Geoinformation 115 (2022) 103124

Contents lists available at ScienceDirect

International Journal of Applied Earth Observations and Geoinformation

journal homepage: www.elsevier.com/locate/jag

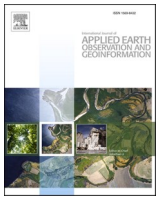

Monitoring winter wheat growth performance at sub-field scale using multitemporal Sentinel-2 imagery

Bing-Bing Goh [a,*], Peter King [b], Rebecca L. Whetton [a], Sheida Z. Sattari [b], Nicholas M. Holden [a]

[a] School of Biosystems and Food Engineering, University College Dublin, Belfield, Dublin 4, Ireland
[b] Origin Enterprises Digital Ltd, HQ Building 329F Wing Thompson Avenue, Harwell Campus, Didcot OX11 0GD United Kingdom

ARTICLE INFO

Keywords:
Precision agriculture
Crop monitoring
Remote sensing
Crop biophysical
Spectral bands
Spatial analysis

ABSTRACT

A crop growth monitoring system should objectively and reproducibly reflect changes in crop biophysical properties during the growing season. By monitoring crop growth and performance at specific crop development stages, the farmer can obtain reliable information for timely crop management to achieve optimum crop production. This work aimed to evaluate crop development using five winter wheat (*Triticum aestivum* L.) biophysical properties (shoots number, green area index, plant height, leaf N content, and aboveground dry biomass) predicted from Sentinel-2 data compared with benchmarks representing target growth from emergence to harvest. Data were collected for four principal phenology stages (tillering, stem elongation, heading, and fruit development) in 35 winter wheat fields in the Republic of Ireland and 40 in the United Kingdom in 2020 and 2021. A total of 1500 plots were selected for crop sampling over two growing seasons. The models were generally good, but phenology-specific models performed better (R^2 between 0.72 and 0.87) than models for the entire season (R^2 between 0.13 and 0.84). To assess the low-performance zones in fields, the predicted biophysical properties were compared to benchmarks taken from agronomic advice. Spatial analysis was then used to identify low-performance areas in fields, which were validated using farmers' feedback. It was concluded that the approach taken could be reliably used to monitor winter wheat over a wide area and through time.

1. Introduction

Crop growth is a quantitative and irreversible process associated with changing plant morphological features leading to an increase in those features that constitute the yield (e.g., grain) (Sadras et al., 2016). Crop growth underperforms (i.e., does not deliver the expected return on investment of husbandry resources and time) when the amount of CO_2 (Farkas et al., 2021), radiation (Mu et al., 2010), water (Fahad et al., 2017), and nutrients (Barraclough et al., 1989), or such inputs are lower than needed to achieve the target yield. Crop growth monitoring before harvest is essential to support husbandry decisions, forecast yield, and understand environmental impacts (Boori et al., 2020). Timely monitoring of crop biophysical properties (CBP) such as leaf area index (LAI), aboveground biomass, crop chlorophyll content, and plant height provides valuable information to understand the crop development, variation in plant morphology, nutrient uptake, and pesticide needs during crop growth (Thorp et al., 2012).

Winter wheat (*Triticum aestivum* L.) is the dominant cereal crop in the Republic of Ireland (IE) and the United Kingdom (UK). Winter wheat is more expensive to grow than spring wheat because the longer growing season requires greater inputs (Fowler et al., 1983; He et al., 2013). To ensure return on investment, regular field scouting is necessary (Evans et al., 2014). As an alternative, satellite remote sensing and geographical information systems (GIS) are the cornerstones of site-specific crop field management, offer the ability to provide information repeatedly over wide areas at low cost. They are the cheapest means of data acquisition and communication for large geographical areas (Skakun et al., 2017), so CBP estimation using remote sensing has been widely developed (Xie et al., 2019). The spectral information obtained from satellite remote sensing has been used to assess plant health and productivity (Y. Wu et al., 2020), chlorophyll content of the leaves (Cui et al., 2019), the green area index (Richter et al., 2012), and the dry aboveground biomass (Du et al., 2015). There has been little research on measuring shoot numbers and plant height using optical spaceborne remote sensing, and the geographical coverage of much works has been restricted to small areas such as experimental plots or adjacent fields (Tao et al., 2020; Wu et al., 2022). This study uses data taken from the plot sampling approach over a wide geographical extent which is not

* Corresponding author.
E-mail addresses: eringohbb@gmail.com, bingbing.goh@ucdconnect.ie (B.-B. Goh).

https://doi.org/10.1016/j.jag.2022.103124
Received 29 July 2022; Received in revised form 18 November 2022; Accepted 20 November 2022
Available online 24 November 2022

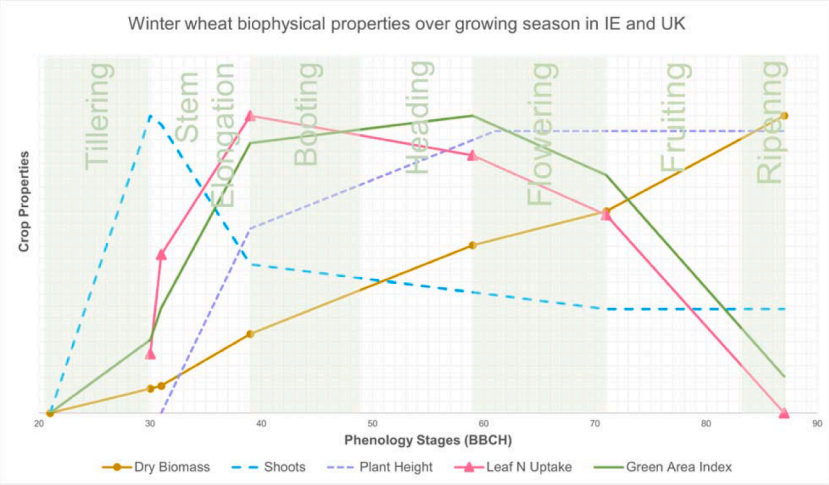

Fig. 1. The change in winter wheat biophysical properties over a typical winter wheat growing season in IE and UK. (compiled using data from: Teagasc (J. Lynch et al., 2016) and (Sylvester-Bradley et al., 2018).

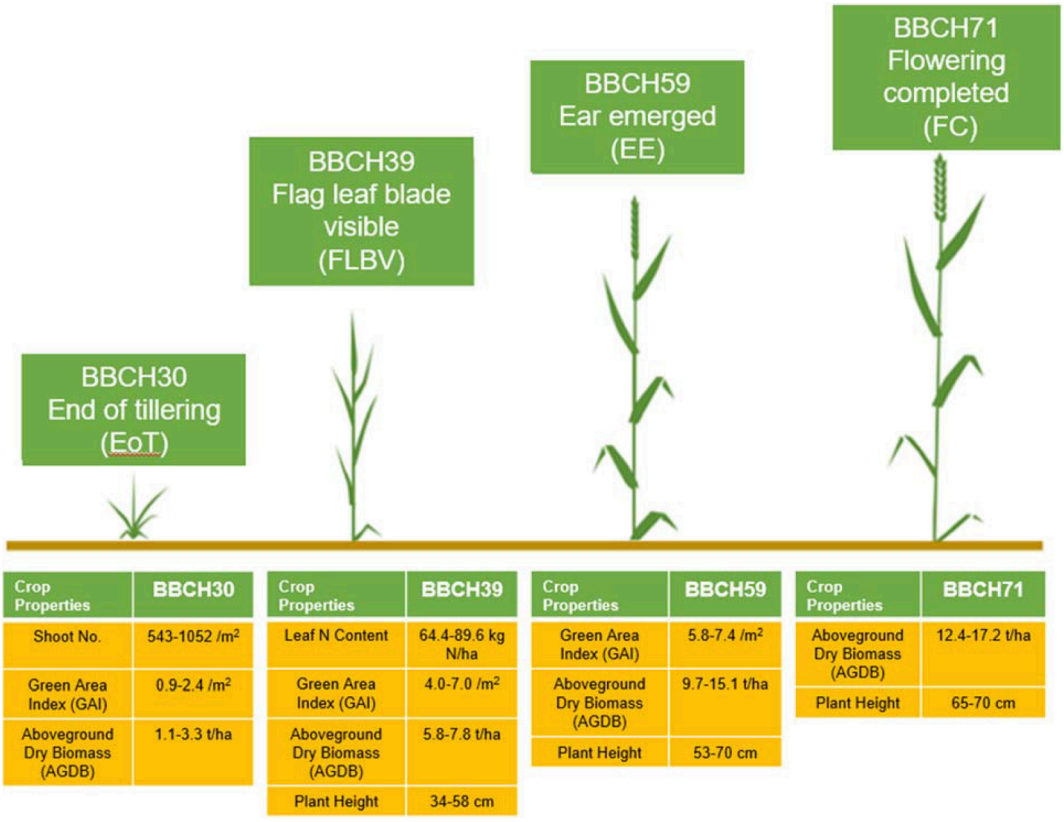

Crop Properties	BBCH30
Shoot No.	543-1052 /m²
Green Area Index (GAI)	0.9-2.4 /m²
Aboveground Dry Biomass (AGDB)	1.1-3.3 t/ha

Crop Properties	BBCH39
Leaf N Content	64.4-89.6 kg N/ha
Green Area Index (GAI)	4.0-7.0 /m²
Aboveground Dry Biomass (AGDB)	5.8-7.8 t/ha
Plant Height	34-58 cm

Crop Properties	BBCH59
Green Area Index (GAI)	5.8-7.4 /m²
Aboveground Dry Biomass (AGDB)	9.7-15.1 t/ha
Plant Height	53-70 cm

Crop Properties	BBCH71
Aboveground Dry Biomass (AGDB)	12.4-17.2 t/ha
Plant Height	65-70 cm

Fig. 2. Benchmark values for CBP at key growth stages for winter wheat growth monitoring derived from Teagasc (J. Lynch et al., 2016) and AHDB (Sylvester-Bradley et al., 2018).

commonly seen in the literature due to a large amount of field labor required.

The aim of this work was to develop the theoretical foundation for a crop growth monitoring system that can be used for winter wheat agronomy services. The concept was to (1) predict the most important biophysical property at a particular growth stage, (2) compare the property to a baseline used by agronomists and farmers for crop management, and (3) map crop relative performance at sub-field level. To achieve this, the objectives of the study were to (1) investigate the use of Sentinel-2 spectral data for estimating shoot number, green area index (GAI), plant height (PH), leaf nitrogen content (LNC), and aboveground dry biomass (AGDB); (2) evaluate the best fit prediction model of these CBP by using two approaches: data for the whole growing season (called full wheat phenology) and data for specific growing time window of CBP (called phenological trait); (3) identify the contribution of each band to estimation of the CBP; (4) prepare CBP maps; and (5) validate the maps by reference to farmer opinion. Ultimately the approach will contribute to a digital crop intelligence system that can help farmers and agronomists achieve optimum winter wheat management.

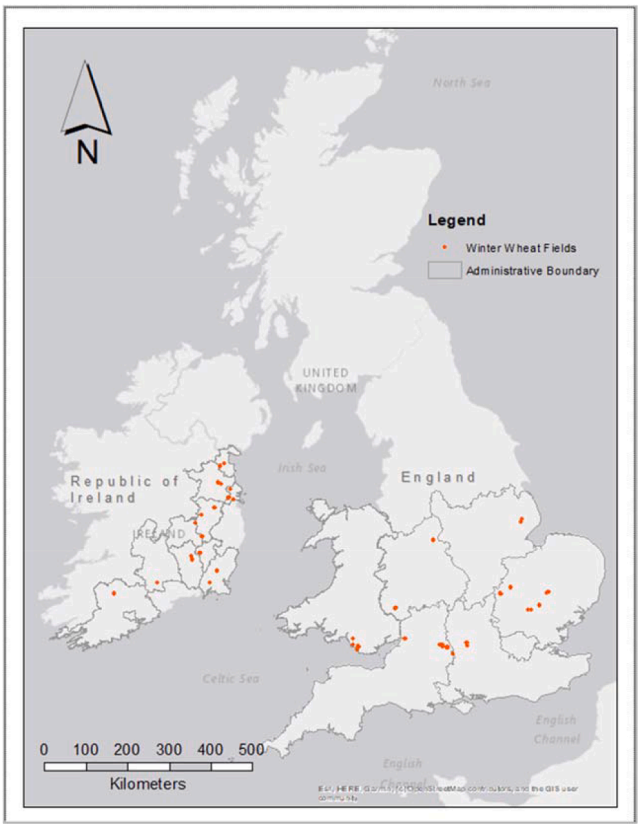

Fig. 3. Locations of 75 winter wheat fields for field sampling in IE and UK.

Table 1
Dataset used in this study for modelling and mapping.

Datasets	Input Data	PLS-R Model	Approaches	Growth Stages
1	Shoot No /Spectral	Shoot	1st	BBCH21-87
2	Shoot No /Spectral	Shoot	2nd	BBCH21-30
3	GAI / Spectral	GAI	1st	BBCH21-87
4	GAI / Spectral	GAI	2nd	BBCH21-59
5	LNC / Spectral	LNC	1st	BBCH30-87
6	LNC / Spectral	LNC	2nd	BBCH30-39
7	PH / Spectral	PH	1st	BBCH31-87
8	PH / Spectral	PH	2nd	BBCH31-71
9	AGDB / Spectral	AGDB	1st	BBCH21-87

2. Theoretical basis for winter wheat growth monitoring

The management decisions for winter wheat are phenological stages dependent, where each stage represents a major change in plant morphology and function (Xue et al., 2004). There are seven key stages: tillering, stem elongation, booting, heading, flowering, fruiting, and ripening (Fig. 1), which can be used to link plant physiology to crop management. Specific crop morphological characteristics change within and between stages (Ledent, 1982). (Fig. 1) illustrates the changes in CBP over a typical winter wheat growing season in IE and UK. The Biologische Bundesanstalt, Bundessortenamt and CHemical industry (BBCH) scale was developed to describe the phenological stages of winter wheat and was used for this work (Lancashire et al., 1991).

In order to place the CBP estimated from Sentinel-2 into a context useful for husbandry, winter wheat growth performance can be assessed against the benchmark values (Fig. 2). These values were derived from data published by Teagasc (Lynch et al., 2016) and AHDB (Sylvester-Bradley et al., 2018) based on observations of optimum yielding winter wheat grown in IE and UK over several growing season. These benchmark values function as quantitative reference points for a comparison with current crop performance. Satellite-derived CBP can then be classified against the benchmark values to create the categories "below target", "on target" and "exceed target". The comparison can be completed at end of tillering (BBCH30), when the flag leaf blade visible (BBCH39), at ear emerged (BBCH59) and when flowering completed (BBCH71). The theory for using the BBCH scale to interpret CBP in the context of winter wheat development is outlined in (Fig. 1). It assumes that the farmer has planned seeding rates and husbandry tactics for a pre-defined target yield (t/ha).

2.1. Shoot number

Following planting, the number of shoots that emerge, and the number of additional tillers after the third leaf has emerged, are important determinants for everything that follows. As seen in (Fig. 1), winter wheat reaches the maximum shoot number around BBCH30 (EoT) and tillering ends just before stem elongation (SE) BBCH31. The shoot number per unit area will determine the potential to develop ears and produce grain. Accurate estimation of shoot number at BBCH30 (EoT) will be useful for fertilizer and chemical input management and whether target yield will be achievable. Monitoring shoot number after BBCH30 (EoT) is less important later in the growing season because it settles after BBCH39 (FLBV). The number of shoots will be influenced by the amount of nitrogen (N) and Phosphorus (P) fertilizer applied (Rodríguez et al., 1998). Engström and Bergkvist (2009) reported a positive relationship between the number of days of spring N application before BBCH30 (EoT) and the number of shoots from beginning of tillering (BoT) BBCH21 to BBCH30 (EoT). There have been few studies on estimating shoot number using ground-based (Fang et al., 2020; Ishikura et al., 2020) and airborne (Roth et al., 2020; Wu et al., 2022) remote sensing, but none using spaceborne remote sensing across large geographical areas.

2.2. Green area index

The GAI describes canopy characteristics related to radiation absorption, evapotranspiration, and crop growth (Bukowiecki et al., 2020). GAI is defined as the projected area of green leaves and stems per unit of ground area. Chikov et al. (2020) have found that the stem, ear and leaf of winter wheat all contribute to photosynthesis, so GAI is thought to be a more useful index than LAI, the area of leaves per unit ground area. LAI can be difficult to measure due to clumping and overlap of leaves (Breda, 2003), and according to Duveiller et al. (2011), GAI is a more pertinent biophysical parameter to retrieve from satellite remote sensing because satellite sensors capture reflectance from the whole crop canopy, not just the leaves. (Fig. 1) shows the development of GAI between BBCH21 (BoT) and BBCH59 (EE). The most rapid change occurs between BBCH31 (SE) and BBCH39 (FLBV), the stem elongation stage as the plant responds to increased radiation and temperature. The increase continues during heading to BBCH59 (EE). In this study, any decline in estimated GAI from BBCH21 (BoT) to BBCH59 (EE) indicates poor performance, perhaps due to foliar disease, drought, or nutrient deficiency. There has been a rapid development of remote sensing technology to derive GAI from spaceborne optical sensors for wheat yield estimation (Kouadio et al., 2012) and crop monitoring (Bukowiecki et al., 2021).

2.3. Plant height

PH characterizes the vertical plant structure, and is important for determining lodging risk (Zhang et al., 2021; Chauhan et al., 2021). PH increases rapidly from BBCH31 (SE) and reaches the maximum height at the end of heading (EoH) at BBCH61 (Fig. 1). Excessive N fertilizer can

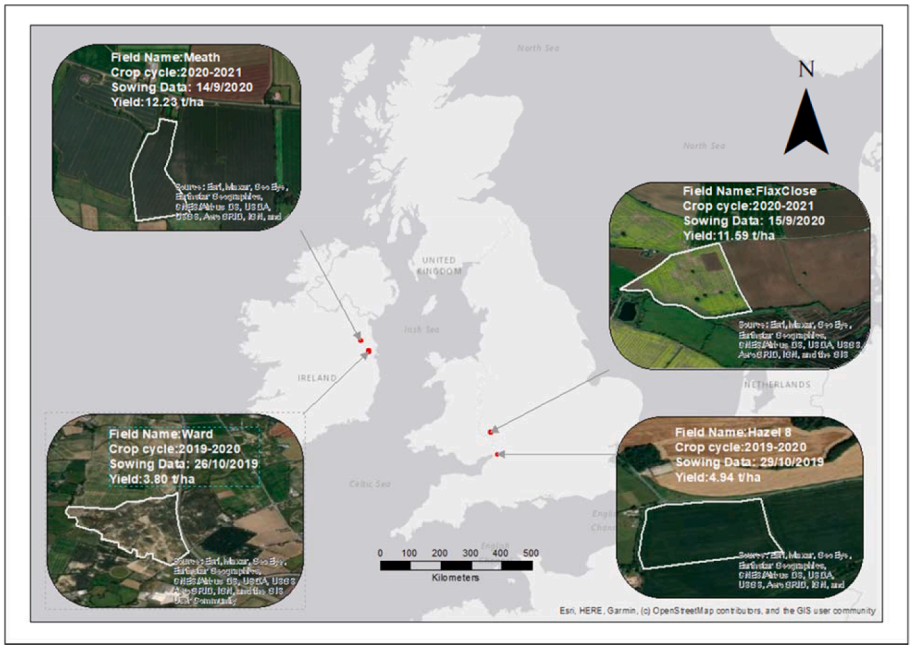

Fig. 4. Location of winter wheat fields selected for crop properties mapping and performance zoning.

Table 2
Winter wheat fields information from IE and UK.

Country	Wheat Field	Crop Cycle	Sowing Date	Yield (t/ha)	Area (ha)
IE	Ward2	2019/20	26/10/2019	3.8	75.8
IE	Meath1	2020/21	14/09/2020	12.2	8.4
UK	Hazel8	2019/20	29/10/2019	4.9	7.8
UK	FlaxClose	2020/21	15/09/2020	11.6	14.1

Table 3
Models for CBP estimation with Sentinel-2 spectral bands and results in training and testing models.

	Training			Testing		
	R^2	RMSE	NRMSE	R^2	RMSE	NRMSE
Shoots per m^2						
BBCH21-87	0.13	220.00	0.14	0.14	200.00	0.19
BBCH21-30	0.77	180.00	0.11	0.86	131.00	0.12
GAI (m^2/m^2)						
BBCH21-87	0.68	1.13	0.17	0.68	1.18	0.18
BBCH21-59	0.85	0.86	0.13	0.87	0.81	0.13
PH (cm)						
BBCH31-87	0.73	8.78	0.13	0.84	6.83	0.12
BBCH31-71	0.72	8.28	0.14	0.75	7.56	0.13
LNC (kg N/ha)						
BBCH30-87	0.54	30.19	0.14	0.56	29.30	0.16
BBCH30-39	0.74	18.99	0.13	0.69	24.75	0.18
AGDB(t/ha)						
BBCH21-87	0.86	3.41	0.11	0.84	3.63	0.13

cause crop lodging, diseases, and pollution. Thus, schedule of early plant growth regulation application is impactful in restricting crop height (J. Lynch et al., 2016). Many studies have used unmanned aerial vehicles (UAV) (Song and Wang, 2019; ten Harkel et al., 2019; Tao et al., 2020) to estimate PH, but few attempts had been made to monitor the wheat PH using the spaceborne remote sensing data (Xu et al., 2010; Chauhan et al., 2019) and to our knowledge none was using Sentinel-2. In this study, estimated PH was used to indicate the continuity of stem elongation at BBCH39 (FLBV), BBCH59 (EE) and BBCH71 (FC).

2.4. Leaf nitrogen content

Nitrogen is a critical component of the enzymes associated with chlorophyll, which enable plants to absorb sunlight and produce sugars from water and carbon dioxide through photosynthesis (Reich et al., 1995). With a better understanding of crop N accumulation, the farmer would be able to regulate N management by applying the appropriate amount at the appropriate time, based crop N demand (Frederick and Camberato, 1995; Jiang et al., 2021). Insufficient N supplies may cause smaller leaves, reduced chlorophyll content and decreased biomass production (Hokmalipour et al., 2011). The greatest rate of leaf N uptake is from BBCH30 (EoT) to BBCH39 (FLBV). During these critical growth stages, if the N supply is less than optimum, the crop will underperform with reduced canopy survival, final ear number, and yield. N uptake is stagnant after the flag leaf emerges and then starts to decline when the crop reaches maximum canopy height and size from BBCH39 (FLBV) to BBCH59 (EE) (Fig. 1). Delloye et al. (2018) found immense potential for using Sentinel-2 for N recommendation during 2nd and 3rd N applications at BBCH30 (EoT) to flag leaf visible still rolled (FLVR) BBCH37. In this study, estimated leaf N uptake was used to assess the leaf N status across a field.

2.5. Above ground dry biomass

AGDB monitoring using remote sensing technique is most common in smart agriculture and precision agriculture as a strong predictor of crop productivity (Marshall et al., 2022). Crop biomass accumulation is driven by the radiation intercepted by the crop, nitrogen supply and available water (Serrano et al., 2000). (Fig. 1*)* shows that by early April, the crops start receiving more sunlight causes the accumulating AGDB to increase rapidly from BBCH31 (SE) due to the development of stems and leaves. At BBCH39 (FLBV), AGDB accumulates further, but this time from the stems, leaves, and ear. The accumulation of AGDB is primarily contributed by stems and ears after BBCH39 (FLBV). More than 50% of AGDB accumulation happens in the ears after BBCH59 (EE). The maximum accumulation of AGDB happens around hard dough (HD) BBCH87 before ear senescence takes place. Numerous studies have focused on estimating plant biomass using spaceborne remote sensing as an operative estimator together with vegetation index models (Gaso et al., 2019; Kokhan & Vostokov, 2020) and evapotranspiration models

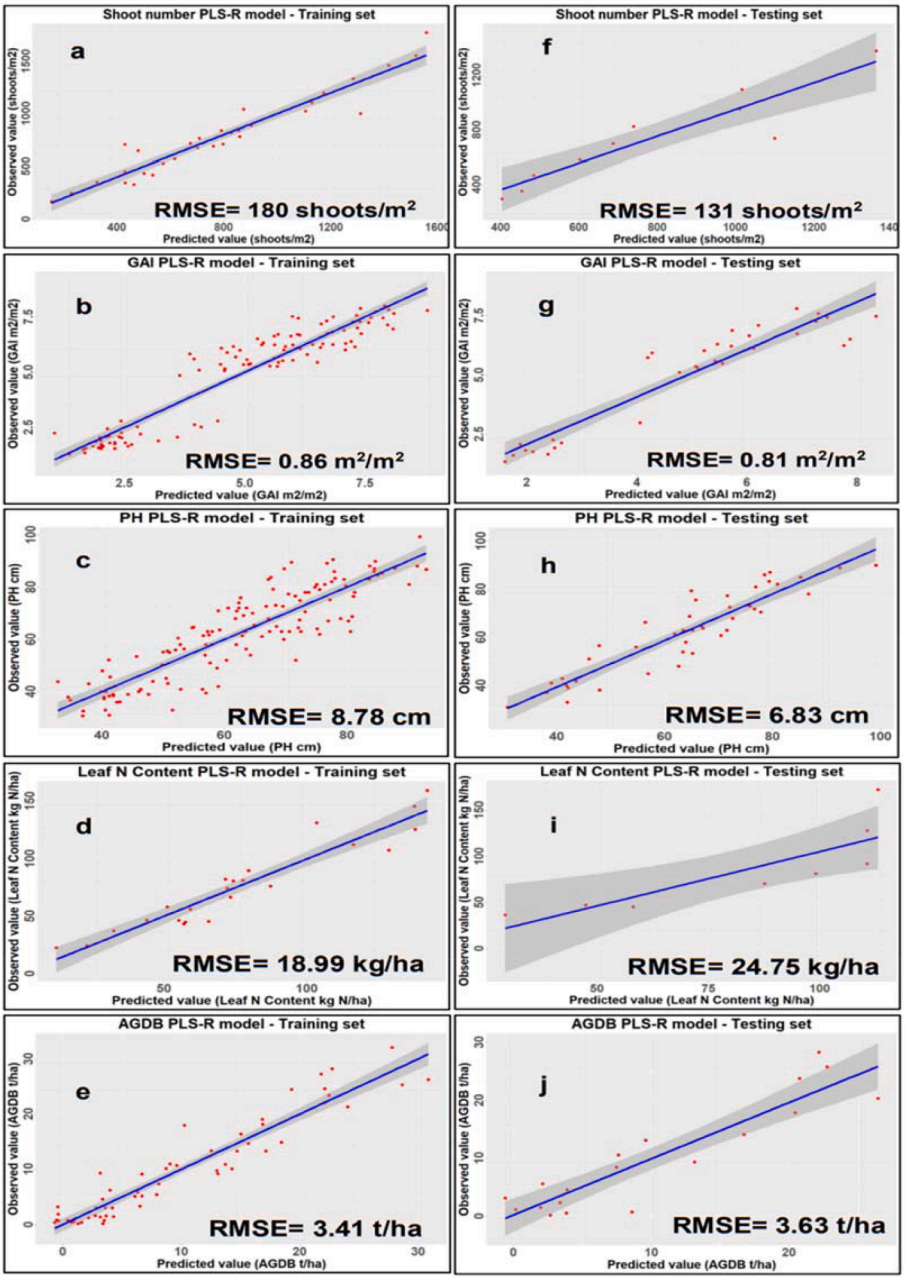

Fig. 5. Plot of observed and predicted values for the 5 optimal PLS-R models for training and testing datasets (a) Plot for shoot number using training dataset (b) Plot for GAI using training dataset (c) Plot for PH using training dataset (d) Plot for LNC using training dataset (e) Plot for AGDB using training dataset (f) Plot for shoot number using testing dataset (g) Plot for GAI using testing dataset (h) Plot for PH using testing dataset (i) Plot for leaf N using testing dataset (j) Plot for AGDB using testing dataset.

(Ouaadi et al., 2020) for crop yield prediction.

3. Materials and methods

3.1. Sampling sites

The study used 35 winter wheat fields in IE and 40 in the UK, with all fields being > 1 ha (Fig. 3). The CBP ground truth were collected during field campaigns between 2019 and 2021 for 2 winter wheat production cycles. All sites fall within a temperate climate with an annual average temperature between 6 and 14 °C, 600 to 1500 mm annual rainfall, and 1200 to 1600 h total annual sunshine. None of these fields had a steep slope of more than a 15% slope gradient (Jarasiunas, 2016).

3.2. Sampling strategy

Sampling was timed using a growing degree day calculator and further confirmation from the farmer to capture four key phenological stages of winter wheat: tillering, stem elongation, heading, and fruiting (Fig. 1). In each field, number of shoots, GAI, leaf chlorophyll content, PH and above ground fresh biomass was sampled from five quadrats disbursed over 1 ha. A random location was picked at least 20 m offset from the field boundary or other disruptions to avoid edge and shadow effects. Sampling started at this location by randomly locating a 0.5 m × 0.5 m quadrat. A further four locations were picked at random, at least 20 to 40 m apart. Each quadrat location was recorded in latitude and longitude. All field observations were taken within the quadrat, which was then destructively sampled for above ground biomass. In total, there were 700 samples taken from Ireland and 800 from the UK each year, making a total of 1500 samples over two years.

3.3. Crop biophysical measurements

At each quadrat location, a downward looking digital photo was

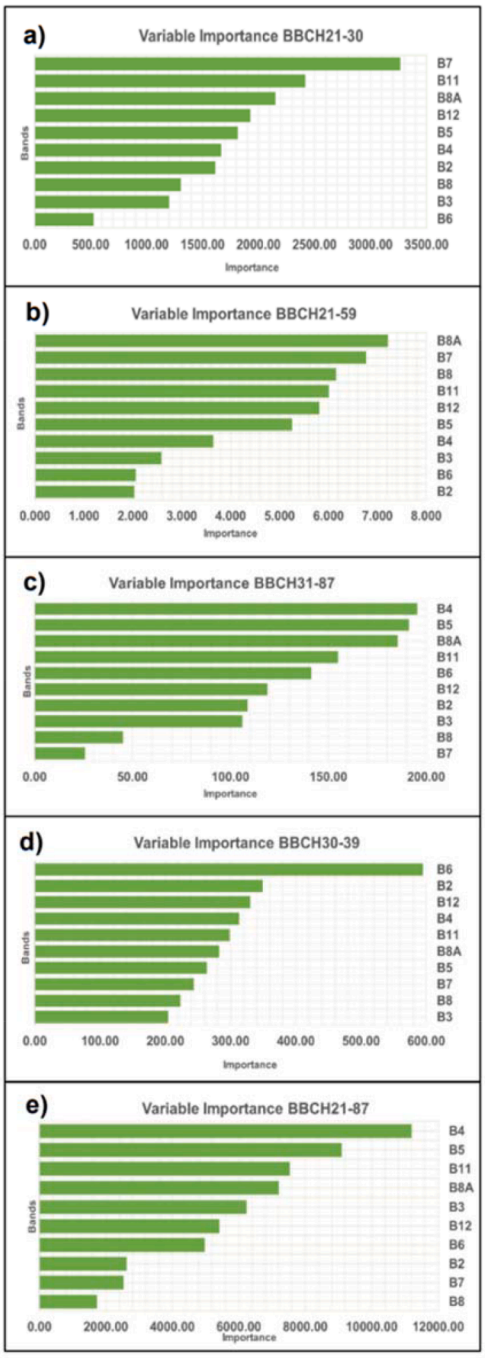

Bands	Spectral Region
B2	Blue
B3	Green
B4	Red
B5	Red-Edge
B6	Red-Edge
B7	Red-Edge
B8	Near Infrared (NIR)
B8A	Narrow (NIR)
B11	Shortwave Infrared (SWIR)
B12	SWIR

Fig. 6. VI of PLS-R models for CBP. (a) VI for shoots number estimation within BBCH21-30. (b) VI for GAI estimation within BBCH21-59 (c) VI for PH estimation within BBCH31-87 (d) VI for LNC estimation within BBCH30-39 (e) VI for AGDB estimation within BBCH21-87.

taken above the crop canopy to record the conditions during sampling. The GAI of the crop within the quadrat were measured using the BASF GAI smartphone application. Leaf chlorophyll content was determined using a Konica Minolta SPAD-502Plus chlorophyll meter as the average of 10 measurements from the uppermost leaves. The leaf nitrogen concentration (LC%) was calculated based on Konica Minolta published equation (*Eq. (1)*) at https://www.konicaminolta.com/instruments.

$$LC\% = 0.079(SPAD) - 0.154 \quad (1)$$

Multiply the value of LC% by leaf dry biomass (LDB) to get the LNC (Li et al., 2018) (*Eq. (2)*).

$$LNC = LDB \times LC\% \quad (2)$$

The specific BBCH code was recorded for each quadrat by matching the crop morphology with the BBCH-scale description. The plants within the quadrat were cut at the ground surface and transported in a labelled plastic bag to the laboratory, where total number of shoots and PH were determined. Finally, the plants were split into leaves, stems and spikes, weighed, and oven dried at 70 °C for 48 h until a constant weight was achieved.

3.4. Farmers' field observations

Field observation notes recorded by the farmers contained general appearance of the crop, foliar disease effects, weeds coverage, insect effects, lodging and stone content. Where the farmer had a reliable

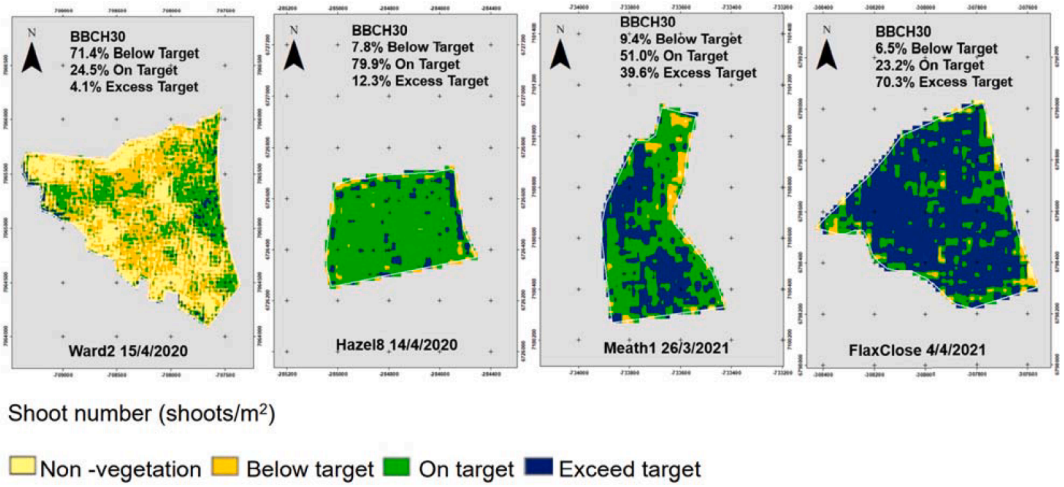

Fig. 7. Crop performance maps derived from estimated shoot number relative to the benchmark value at BBCH30 (EoT).

record of field notes, these were collected and used to validate the crop performance maps.

3.5. Sentinel-2 data pre-processing

Cloud and cloud shadow free data from Sentinel-2A and Sentinel-2B were collected between 4 days before and 4 days after the field sampling at each location. The data closest to the sampling date were used for modelling. The Level-2A product, which provides the bottom of Atmosphere reflectance was acquired using Google Earth Engine (GEE). From the 13 spectral bands, Band 1 (Coastal aerosol), Band 9 (Water vapor) and Band 10 (SWIR-Cirrus) were excluded from the analysis. The 10 spectral bands sensitive to vegetation were resampled at a 10 m spatial resolution for further analysis.

3.6. Multivariate regression models

Partial Least Square Regression (PLS-R) is proven to be successful for quantifying vegetation properties using remote sensing data (Ali et al., 2019). The non-parametric, PLS-R method was used with the 10 spectral bands as predictors and the shoot number, GAI, PH, LNC, AGDB as response variables. Each CBP for each field per visit was used as an input to the regression model. The average of each of the 10 spectral bands, for the five pixels aligned to the five quadrats per field per visit were the input data for the regression models. As shown in (Table 1), these input data were further sorted by CBP and growth stage to construct 9 different datasets for modelling.

PLS-R models were developed using two approaches for each CBP except AGDB. The first approach, called full wheat phenology, measured the association between CBP and spectral bands over all stages of crop growth. However, the second approach, called phenological trait, measured the association between CBP and spectral bands only during growth stages when the crop properties contributed to significant change in morphology of the plant. It should be noted that AGDB was developed using the first approach only because AGDB should increase for all crop growth stages as illustrated in (Fig. 1*)*. *T*he AGDB model was constructed using only the IE data because of data quality issues associated with ovens drying of UK samples caused by COVID-19 restrictions leading to excessive transport distances and storage times.

In order to achieve a high prediction ability model, there were several configurations that could be used, such as leave-one-out cross validation and setting for wide kernel PLS algorithm while the number of variables was larger than the number of observations (Liland et al., 2020). The models were evaluated further using train-test split approach with 80% samples as training dataset and 20% samples as testing dataset. The best PLS-R component based on the greatest coefficient of determination (R^2), the smallest root mean square error (RMSE), and normalized root mean square error (NRMSE) close to zero was selected to ensure the most appropriate model (Yue et al., 2018).

3.7. Commonly used vegetation indexes

Commonly used vegetation indexes such as normalized difference vegetation index (NDVI) and enhanced vegetation index (EVI) were found not satisfactory in predicting the five crop biophysical properties in this study. For detailed information, see the supplementary data or supporting information. The most common issues of NDVI are saturation of its value in a dense vegetation area (Aparicio et al., 2000) and interference from soil reflectance at low crop densities (Mulla, 2013). Furthermore, the NDVI and EVI values do not have a uniquely predictive relationship with specific biophysical properties, so it can be difficult to untangle and identify exactly which properties are causing a given NDVI and EVI values at a given time and location.

3.8. Mapping crop growth performance

A spatial distribution map of each CBP derived from the five best CBP models was created using the map algebra in ArcGIS Pro (Version 2.8.7). For preliminary evaluation, four winter wheat fields in (Fig. 4*)* were selected*, two* from the IE and two from the UK. The four fields were selected based on two having high yielding crop yield > 10 t/ha, which is considered as good yielding crops in IE and UK (Lynch et al., 2017; Sylvester-Bradley et al., 2018) and two having low crop yield in each country. These selected fields were excluded from the train and test models development. The details of the four winter wheat fields are provided in (Table 2*)*. The CBP of the four winter wheat fields were estimated using the optimum PLS-R models in (Table 1*)* and classified relative to the benchmark values in (Fig. 2*)*. Sentinel-2 was used to map spatial variability in crop growth performance of 4 fields at BBCH30 (EoT), BBCH39 (FLBV), BBCH59 (EE), and BBCH71 (FC) and the maps were then validated with farmers' field observation records.

4. Results

4.1. Performance of spectral bands for estimating crop properties using PLS-R

*(*Table 3*)* shows the performance of the CBP for full wheat phenology and phenological trait models. All five CBP of winter wheat correlated positively with the spectral bands. The shoot number estimation model

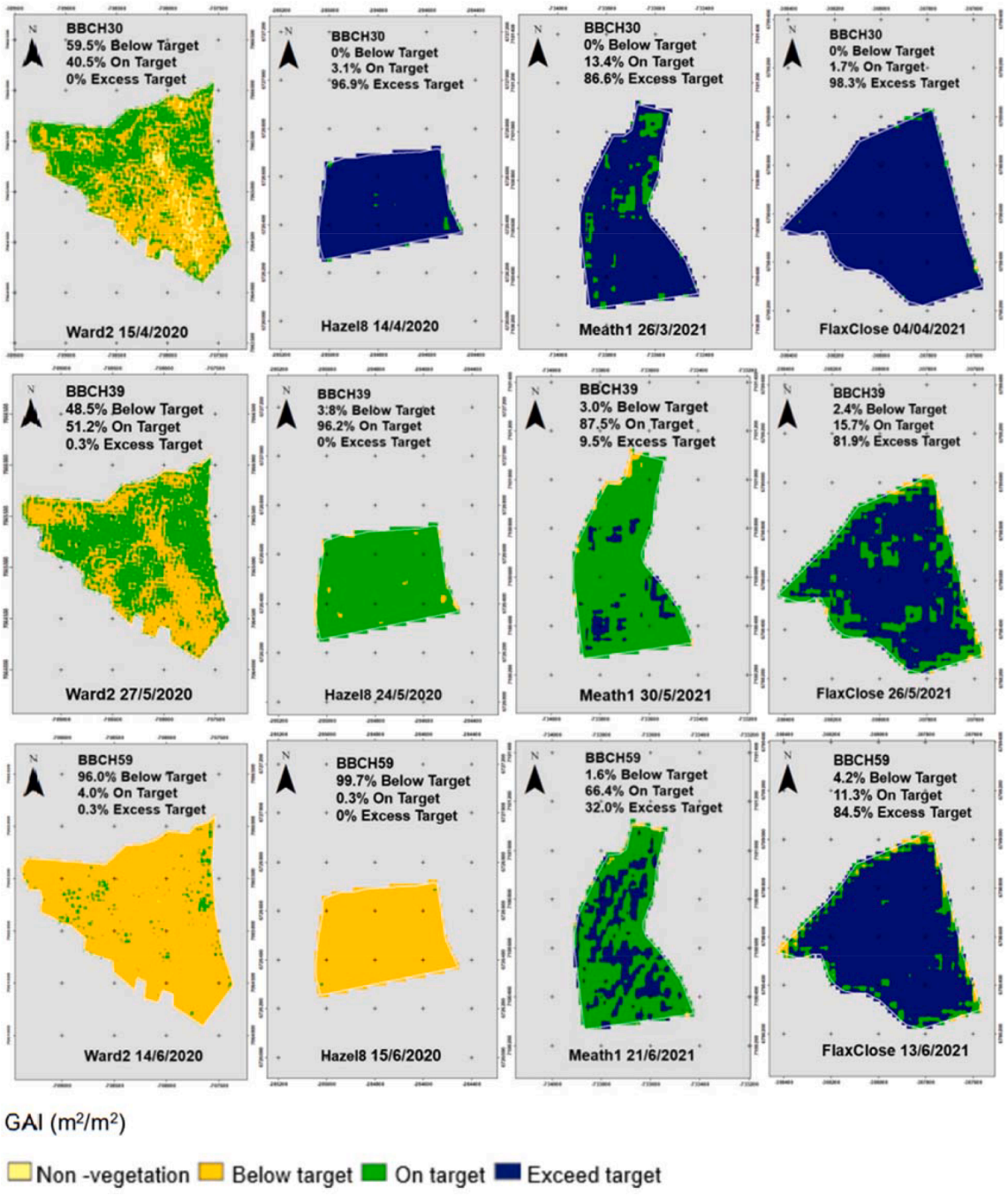

Fig. 8. Crop performance maps derived from estimated GAI relative to the benchmark value at BBCH30 (EoT), BBCH39 (FLBV) and BBCH59 (EE).

based on full wheat phenology (BBCH21-87), showed the weakest correlation, with a RMSE of 220 tillers/m^2 making it unusable for management decision making. Focusing on the phenological trait for this growth period, the RMSE reduced to 180 tillers/m^2. In this study, we found that except for PH, the phenological trait models performed better than the full wheat phenology models. The study also indicated that AGDB and GAI were the two CBP that best associate with the spectral bands with $R^2 = 0.86$ and $R^2 = 0.85$. Among the testing models, GAI performed best prediction ($R^2 = 0.87$, RMSE = 0.81 m^2/m^2, NRMSE = 0.13). LNC scored weakest prediction ($R^2 = 0.69$, RMSE = 24.75 kg N/ha, NRMSE = 0.18).

4.2. Uncertainty of the five best performance PLS-R models

(Fig. 5*)* displays the predicted against observed plots with the grey shaded area around line of best fit in the graphs presented lower and upper halves of 95% confidence interval. Narrower confidence intervals increased precision of the model and decreased prediction error. It can be observed from (Fig. 5*a - j*) that the sample size affects the widths of the confidence intervals. (Fig. 5*b & g)* show underestimated GAI values when observed GAI < 3.8 m^2/m^2 in training model and when observed GAI < 5.0 m^2/m^2 in testing model. Significant overestimated GAI values are discovered in Fig. 5*g* when observed GAI between 5.0 – 7.5 m^2/m^2.

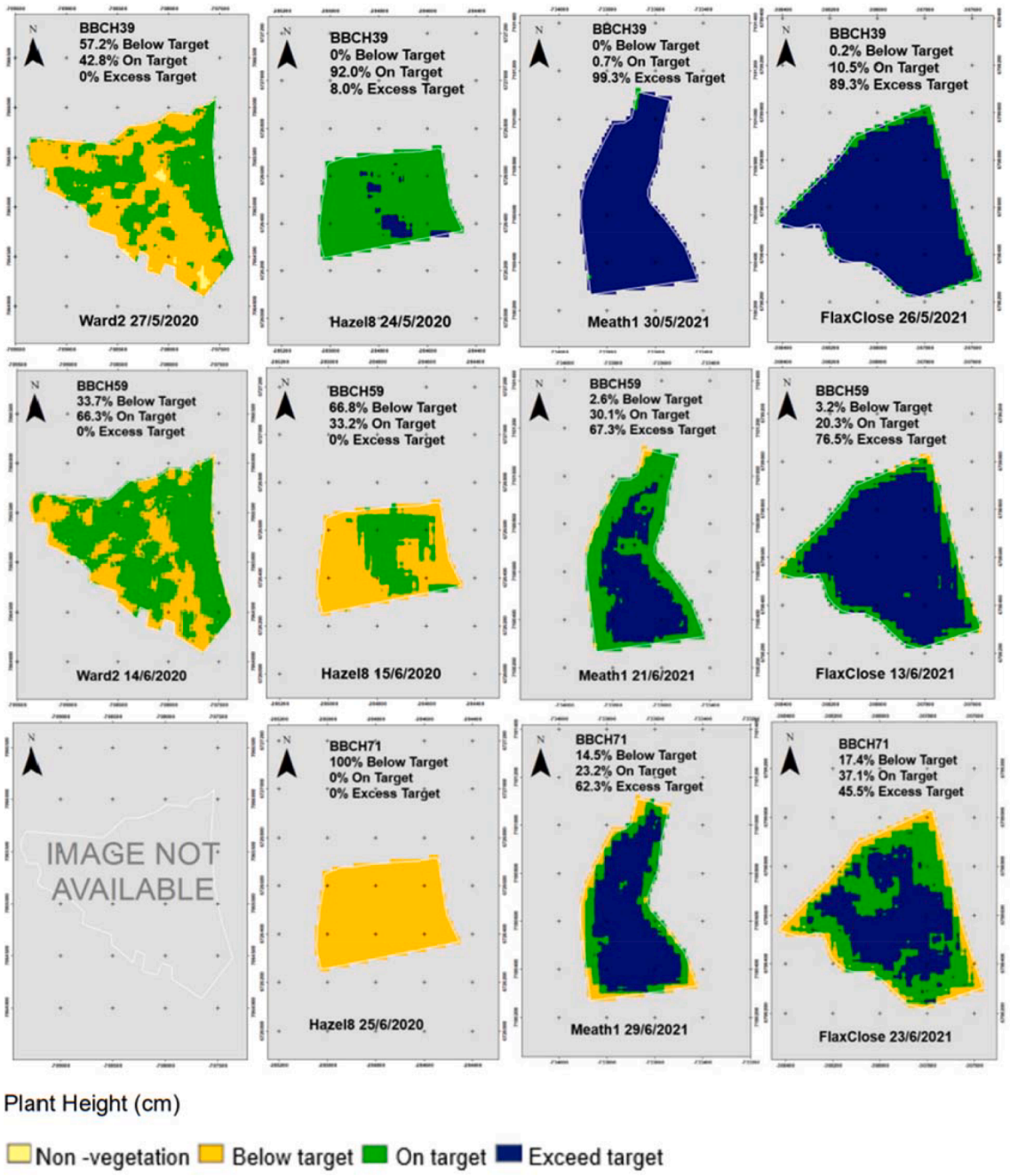

Fig. 9. Crop performance maps derived from estimated PH relative to the benchmark value at BBCH39 (FLBV), BBCH59 (EE) and BBCH71 (FC).

4.3. Variable importance of the five best performance PLS-R models

Variable Importance (VI) of PLS-R models for CBP estimation help to create accurate predictions. The more a model depends on a variable, the more important it is in prediction. *(*Fig. 6*a-e)* shows the ranking of the VI for the five best PLS-R models. Based on these data, the red edge bands B5, B6, B7 and the short-wave infrared (SWIR) B11, B12 have a significant contribution to all five models. Near infrared (NIR) B8, B8A played important roles in shoot number, GAI, PH and AGDB models as well. Visible blue (B2) was a top five contributor for the LNC model, visible green (B3) for the AGDB model and visible red (B4) for the LNC, AGDB and PH models.

4.4. Spatial distribution maps of crop growth performance.

4.4.1. Shoot number growth performance map

The estimated shoot number from the four winter wheat fields in (Fig. 4) was mapped for BBCH30 (EoT). The estimated value was compared relative to the benchmark values 543–1052 per m^2 in *(*Fig. 2) to create crop performance map as in (Fig. 7). Among the four fields, Hazel8, Meath1 and FlaxClose show the overall good crop performance with 92%, 91%, and 94% respectively of the field area are on target or exceeding target at this stage of crop development. In Ward2 field 71% of the crop area did not reach the benchmark value of at least 543 shoots/m^2.

4.4.2. Green area index growth performance map

In *(*Fig. 8*)*, Hazel8, Meath1 and FlaxClose show good crop

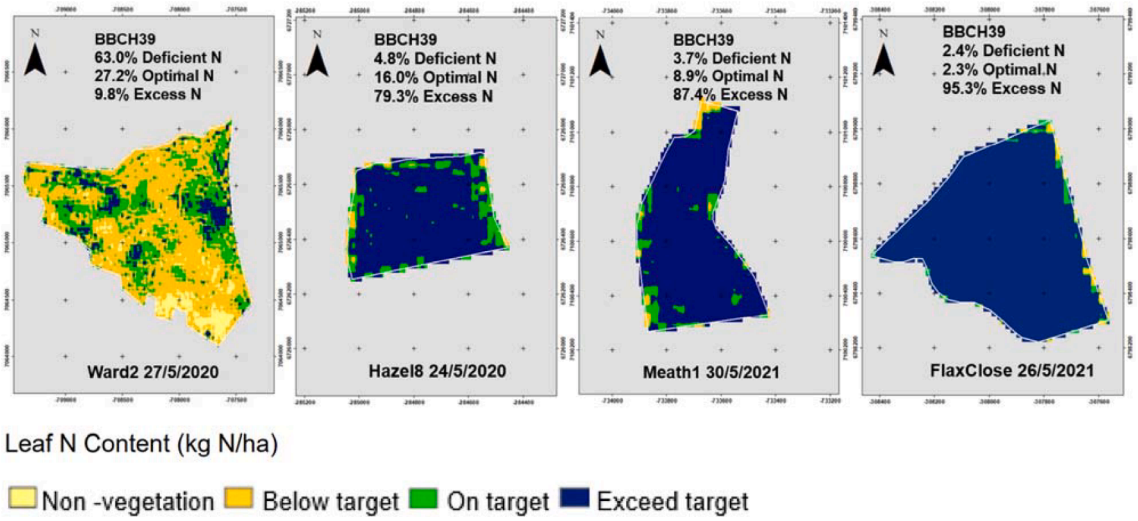

Fig. 10. Crop performance maps derived from estimated LNC relative to the benchmark value at BBCH39 (FLBV).

performance. There were 0% of crops falling below target for achieving good yield. Conversely, more than 50% of the crop area in Ward2 were lower than the benchmark value of 0.9 m^2/m^2 (Fig. 2). Ward2 showed a slight increase in crop performance with crops on target relative to benchmark GAI values of 4.0–7.0 m^2/m^2 at BBCH39 (FLBV) from 40% to 51%. Taking a closer look at Hazel8 and Meath1, majority of the crop area was on target for good yield at BBCH39 (FLBV). FlaxClose continued to maintain crop development with 82% of the field exceeding GAI = 7 m^2/m^2. At BBCH59 (EE) when the canopy reaches maximum size, there was a substantial change observed in Hazel8. The crop performance plummeted to > 99% below the targeted GAI value of 5.8–7.4 m^2/m^2(Fig. 2). While the crop performance in Ward2 showed no improvement and 96% of crops did not achieve GAI values of 5.8 m^2/m^2 at this stage. Meath1 and FlaxClose appeared to have stable crop performance up to this stage.

4.4.3. Plant height growth performance map

(Fig. 9) revealed the distinct variation among the four fields at BBCH39 (FLBV), BBCH59 (EE) and BBCH71 (FC). Overall result showed that crops in Meath1 and FlaxClose performed well at BBCH39 (FLBV), BBCH59 (EE) and BBCH71 (FC). Meath1 performed the best with 100%, 97% and 86% of crop area achieving benchmark values of 34–58 cm, 53–70 cm, 65–70 cm at three specified growth stages respectively (Fig. 2). FlaxClose achieved > 99%,97% and 83% of crop area achieving the benchmark height at BBCH39 (FLBV), BBCH59 (EE) and BBCH71 (FC). In contrast, Ward2 and Hazel8 had poor crop performance. Hazel8 initially has good crop condition at BBCH39 (FLBV) with 92% of crops on target and 8.0% of crops exceeding target PH. The performance reduced (Fig. 9) at BBCH59 (EE) and BBCH71 (FC). Ward2 consistently had poor crop performance with 43% and 66% of crop area on target of 34–58 cm PH at BBCH39 (FLBV) and 53–70 cm at BBCH59 (EE). No Sentinel-2 image was available at BBCH71 (FC) for Ward2 due to cloud cover.

4.4.4. Leaf N content performance map

LNC performance map (Fig. 10) will keep the farmer informed of the crop N status after the 3rd N split application at BBCH37 (FLVR). The LNC distribution pattern of Ward2 was consistent with the other crop properties (GAI, PH) already presented. About 63% of crop in Ward2 underperformed with leaf N deficiency below the benchmark value of 64.4–89.6 kg N/ha in (Fig. 2). Compared to Ward2, Hazel8, Meath1 and FlaxClose had only 5%, 4% and 2% of crop leave N deficiency at BBCH39 (FLBV). FlaxClose had the highest percentage of crops (95%) exceeding the benchmark of 89.6 kg/ha in (Fig. 2).

4.4.5. Aboveground dry biomass performance map

The AGDB crop performance distribution maps (Fig. 11) show, at the beginning of the crop development, significant variation of AGDB performance between Ward2, Hazel8, Meath1 and FlaxClose. Hazel8, Meath1 and FlaxClose had 99%, 100% and 99% respectively on par and exceeding the AGDB benchmark values of 1.1 – 3.3 t/ha in (Fig. 2) at BBCH30 (EoT). Ward2 had 90% of crop area below 1.1 t/ha. Moving forward to BBCH39 (FLBV), the AGDB performance maps reveal good performance of Hazel8, Meath1 and FlaxClose but not for Ward2. Similar to the GAI and PH, the AGDB performance of Hazel8 takes a downward trend from 99% of crops achieving 1.1–3.3 t/ha AGDB at BBCH39 (FLBV), to 97% achieving 5.8–7.8 t/ha AGDB at BBCH39 (FLBV) but only 3% achieving 9.7–15.1 t/ha at BBCH59 (EE) and 0% of crops achieve 12.4–17.2 t/ha at BBCH71 (FC). Ward2 had downward trend at BBCH39 (FLBV) with only 2% of crop area reaching the target AGDB but shows sign of increment at BBCH59 (EE) with 42% of crops reaching at least 9.7 t/ha.

5. Discussion

5.1. The performance of Sentinel-2 for crop biophysical properties estimation

The correlation between the CBP of winter wheat and the Sentinel-2 spectral bands showed strong relationships at the growth stages when the CBP contribute to significant change in plant morphology. This is because the satellite sensors received reflectance from the green canopy including all plant organs namely leaf, stem and ear that are photosynthetically active (Duveiller et al., 2011). As in (Fig. 1), even though some CBP such as shoots and LNC have stopped increasing at BBCH30 (EoT) and BBCH39 (FLBV) respectively, other crop properties including GAI, PH and AGDB continuing to increase and are the fundamental traits contributing to canopy reflectance patterns (Segarra et al., 2020).

In the current work, the contribution of the spectral bands in Sentinel-2 to estimate shoot number, GAI, LNC, PH and AGDB showed that red-edge and SWIR were the most effective bands for all five CBP (Fig. 6). (L. Liu et al., 2004) observed that red edge has strong positive correlation with plant water content and canopy chlorophyll density. While (Y. Liu et al., 2021) found that SWIR has a relatively high sensitivity to the soil moisture and bare soil. Chlorophyll *a* and b are the dominant pigments in the leaf chlorophyll. Chlorophyll *a* absorbs maximum light from the red region, band 4 of Sentinel-2, while Chlorophyll *b* reaches peak absorption in the blue region, band 2 of Sentinel-2 (Milne et al., 2015). This is consistent with the result shown in

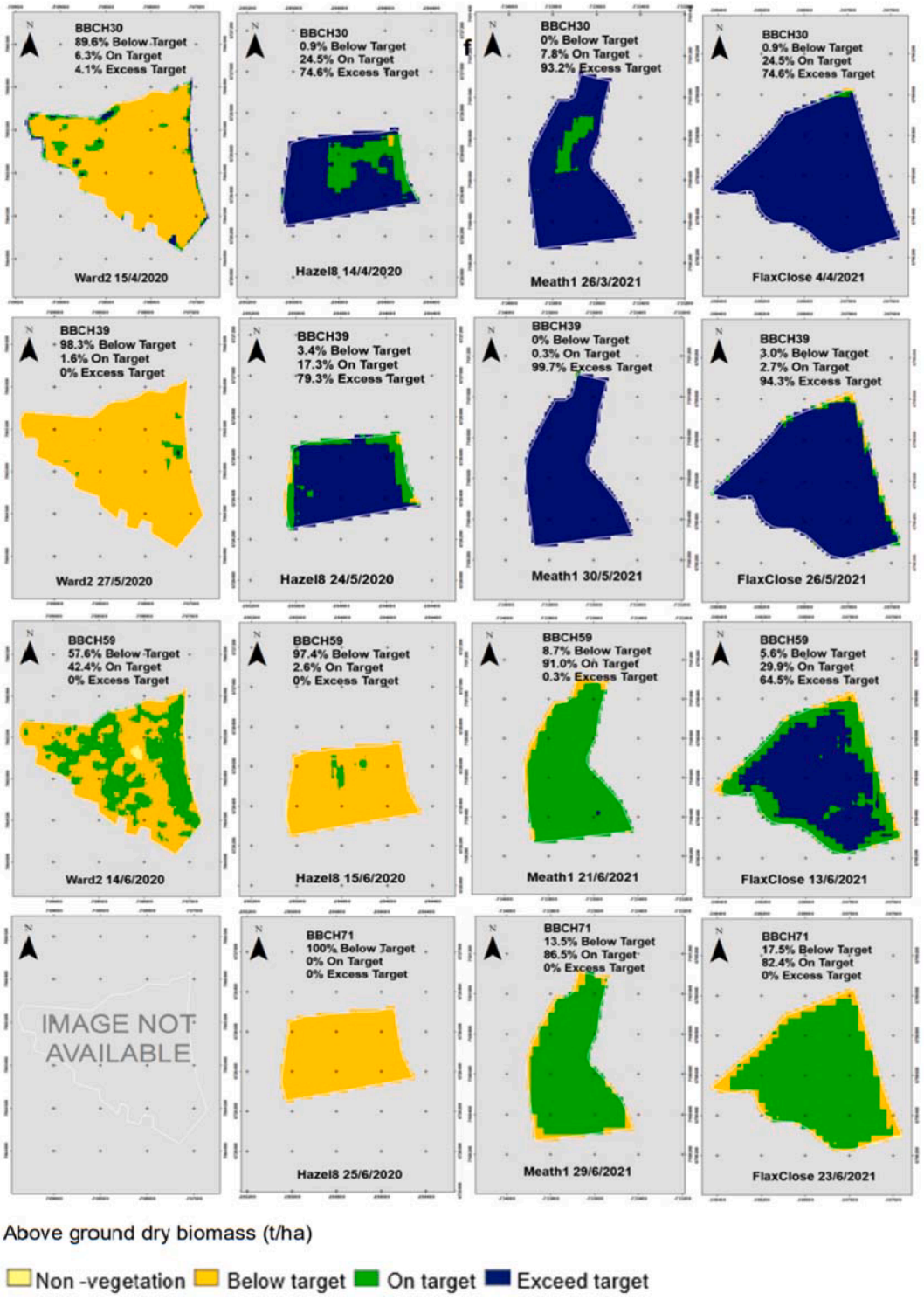

Fig. 11. Crop performance maps derived from estimated AGDB relative to the benchmark value at BBCH30 (EoT), BBCH39 (FLBV), BBCH59 (EE), BBCH71 (FC).

(Fig. 6*d)* where band 2 and 4 are the major contributors to the LNC model. Another influential visible band for the AGDB model was green (band 3). The absorbance in band 3 is due to the anthocyanin (Zahir et al., 2022). The anthocyanin pigment of plants acts as important plant tissue protector against abiotic stressors such as extreme temperature, deficient or excessive water, and mineral deficiency.

Segarra et al. (2020) showed that a combination of spectral indices allows more advance measurement taking into account the robustness of Sentinel-2′s design, specifically for precision agriculture and vegetation monitoring. Our data support this contention.

5.2. Crop biophysical property performance distribution maps

The low shoot number of Ward2 raised the concern of insufficient plant establishment or P and N status at 1st N split (Wang et al., 2021). From the field notes, the farmer identified that Ward2 had poor plant establishment due to the plant seeds being flushed away by heavy rain in November 2019 and February 2020. However, at BBCH59 (EE), there

was an inconsistent distribution pattern between GAI with AGDB and PH. This could reflect a regrowth of the winter wheat crop and chlorosis as reported in photos and observation notes. A severe drought hit the Hazel8 field around middle of heading (MoH) BBCH55 (validated the underperformance CBP from BBCH59 (EE). The crops were stressed and most of the tillers and leaves had dropped according to the farmer's observation. In addition, *Septoria* attacked Hazel8 explaining decreases in AGDB, PH and GAI. Ruan et al. (2021) suggested that foliar diseases destroy pigment, reduce biomass and water content, which explains the results in this case. Unlike Ward2 and Hazel8, Meath1 and FlaxClose performed very well to meet the target for each CBP and achieve a good yield. After the harvest, the yield information was reported by the farmers from each field. Final grain yield of Ward2 and Hazel8 were 3.8 t/ha and 4.9 t/ha which are very low yields. Meath1 and FlaxClose had good yields of 12.2 t/ha and 11.6 t/ha. Sentinel-2 data was capable of being used to estimate the CBP and identify crop growth underperformance. The underperforming zones could be detected well before harvest as they occurred, and the combination of properties provides insight into likely causes. To date, within-field crop growth performance mapping based on the combination of crop properties have not been sufficiently explored. These CBP performance maps could be a reliable source of within-field yield mapping.

5.3. *The limitation of the study and suggestion for future work.*

The Sentinel-2 CBP PLS-R models for winter wheat were able to estimate the CBP at a sub field scale. It was demonstrated that the accuracy of the CBP estimation depended on the prediction time window. In most cases, a phenological trait approach was most effective. Further investigation is needed to create a larger dataset allowing sufficient samples for smaller time windows. Besides increasing the sample size, the uncertainty of the GAI PLS-R model in this experiment could be improved through configuration of digital photos for ground truth GAI (Baret et al., 2010). The generalization of the model was examined by using both IE and UK data that represent variation in environment conditions, climate and soil. Future studies to incorporate new winter wheat field data to account for a wider geographical extent with variety in season, soil, wheat varieties, and multiple years will improve the generalization of model further. Another challenge of using Sentinel-2 to estimate the CBP is cloud cover. At Ward2 field, there was no image available from beginning of flowering (BoF) BBCH60 until harvest. An alternative solution would be to explore Synthetic Aperture Radar data from Sentinel-1 (Khabbazan et al., 2019).

6. Conclusions

Crop growth monitoring is an important input for crop management decision making. Through measurable CBP such as shoot number, GAI, AGDB, leaf N uptake, and crop height, crop growth condition can be monitored thoroughly. Remote sensing is an efficient non-destructive method to retrieve the CBP. This study has shown that models with sufficient accuracy can be developed for the necessary biophysical properties. These can usefully be combined to provide management insights This valuable information will help farm managers to plan crop husbandry strategies. This study showed the potential of using Sentinel-2 with spectral signature modelling to detect the crop morphological change related to shoot number, GAI, AGDB, LNC and AGDB independently of geographical location, climatic zone, soil type and crop genotype (within the area of the British Isles). Using Sentinel-2, the prediction models are more accurate with the phenological trait approach than modelling the full phenology from tillering to ripening. Cloud cover and shadow are key factors that will limit the temporal resolution of support services that might be developed using the approached presented. Among the 10 spectral bands, red edge (Band 5, 6, 7) played a significant role in all the crop biophysical prediction models. Future work should evaluate the robustness of the approach over larger areas and multiple years, testing for different climatic zones, larger numbers of winter wheat varieties, soil types and environmental conditions.

CRediT authorship contribution statement

Bing-Bing Goh: Conceptualization, Methodology, Software, Validation, Formal analysis, Investigation, Data curation, Writing – original draft. **Peter King:** Investigation, Writing – review & editing. **Rebecca L. Whetton:** Investigation, Writing – review & editing. **Sheida Z. Sattari:** Writing – review & editing. **Nicholas M. Holden:** Conceptualization, Investigation, Writing – review & editing, Supervision, Funding acquisition.

Declaration of Competing Interest

The authors declare that they have no known competing financial interests or personal relationships that could have appeared to influence the work reported in this paper.

Acknowledgements

This research has been undertaken as part of the strategic partnership program between Science Foundation Ireland and ORIGIN Enterprises Limited, CONSUS funded under Grant Number 16/SPP/3296. We thank Andy Doyle, Robbie Byrne, and Lucy Cottingham for liaising with farmers in IE and UK.

Appendix A. Supplementary data

Supplementary data to this article can be found online at https://doi.org/10.1016/j.jag.2022.103124.

References

Ali, A.M., Darvishzadeh, R., Shahi, K.R., Skidmore, A., 2019. Validating the Predictive Power of Statistical Models in Retrieving Leaf Dry Matter Content of a Coastal Wetland from a Sentinel-2 Image. Remote Sens. (Basel) 11 (16), Article 16. https://doi.org/10.3390/rs11161936.

Aparicio, N., Villegas, D., Casadesus, J., Araus, J.L., Royo, C., 2000. Spectral Vegetation Indices as Nondestructive Tools for Determining Durum Wheat Yield. Agron. J. 92 (1), 83–91. https://doi.org/10.2134/agronj2000.92183x.

Baret, F., de Solan, B., Lopez-Lozano, R., Ma, K., Weiss, M., 2010. GAI estimates of row crops from downward looking digital photos taken perpendicular to rows at 57.5° zenith angle: Theoretical considerations based on 3D architecture models and application to wheat crops. Agric. For. Meteorol. 150 (11), 1393–1401. https://doi.org/10.1016/j.agrformet.2010.04.011.

Barraclough, P.B., Kuhlmann, H., Weir, A.H., 1989. The Effects of Prolonged Drought and Nitrogen Fertilizer on Root and Shoot Growth and Water Uptake by Winter Wheat. J. Agron. Crop Sci. 163 (5), 352–360. https://doi.org/10.1111/j.1439-037X.1989.tb00778.x.

Boori, M.S., Choudhary, K., Kupriyanov, A.V., 2020. Crop growth monitoring through Sentinel and Landsat data based NDVI time-series. Comput. Opt. 44 (3) https://doi.org/10.18287/2412-6179-CO-635.

Breda, N.J.J., 2003. Ground-based measurements of leaf area index: A review of methods, instruments and current controversies. J. Exp. Bot. 54 (392), 2403–2417. https://doi.org/10.1093/jxb/erg263.

Bukowiecki, J., Rose, T., Ehlers, R., & Kage, H. (2020). High-Throughput Prediction of Whole Season Green Area Index in Winter Wheat With an Airborne Multispectral Sensor. Front. Plant Sci., 10. https://www.frontiersin.org/article/10.3389/fpls.2019.01798.

Bukowiecki, J., Rose, T., Kage, H., 2021. Sentinel-2 Data for Precision Agriculture?—A UAV-Based Assessment. Sensors 21 (8), 2861. https://doi.org/10.3390/s21082861.

Chauhan, S., Darvishzadeh, R., van Delden, S.H., Boschetti, M., Nelson, A., 2021. Mapping of wheat lodging susceptibility with synthetic aperture radar data. Remote Sens. Environ. 259, 112427 https://doi.org/10.1016/j.rse.2021.112427.

Chauhan, S., Srivastava, H.S., Patel, P., 2019. Crop Height Estimation Using RISAT-1 Hybrid-Polarized Synthetic Aperture Radar Data. IEEE J. Sel. Top. Appl. Earth Obs. Remote Sens. 12 (8), 2928–2933. https://doi.org/10.1109/JSTARS.2019.2919604.

Chikov, V.I., Akhtyamova, G.A., Solovyev, D., Burygin, G., 2020. Participation of stem and ear photosynthesis in formation of the crop and its quality in wheat. BIO Web of Conferences 23, 01001.

Cui, B., Zhao, Q., Huang, W., Song, X., Ye, H., Zhou, X., 2019. Leaf chlorophyll content retrieval of wheat by simulated RapidEye, Sentinel-2 and EnMAP data. J. Integr. Agric. 18 (6), 1230–1245. https://doi.org/10.1016/S2095-3119(18)62093-3.

Delloye, C., Weiss, M., Defourny, P., 2018. Retrieval of the canopy chlorophyll content from Sentinel-2 spectral bands to estimate nitrogen uptake in intensive winter wheat cropping systems. Remote Sens. Environ. 216, 245–261. https://doi.org/10.1016/j.rse.2018.06.037.

Du, X., Li, Q., Dong, T., Jia, K., 2015. Winter wheat biomass estimation using high temporal and spatial resolution satellite data combined with a light use efficiency model. Geocarto International 30 (3), 258–269. https://doi.org/10.1080/10106049.2014.937467.

Duveiller, G., Weiss, M., Baret, F., Defourny, P., 2011. Retrieving wheat Green Area Index during the growing season from optical time series measurements based on neural network radiative transfer inversion. Remote Sens. Environ. 115 (3), 887–896. https://doi.org/10.1016/j.rse.2010.11.016.

Engström, L., Bergkvist, G., 2009. Effects of three N strategies on tillering and yield of low shoot density winter wheat. Acta Agriculturae Scandinavica, Section B - Plant Soil Science 59 (6), 536–543. https://doi.org/10.1080/09064710802434363.

Evans, E.W., Carlile, N.R., Innes, M.B., Pitigala, N., 2014. Infestation of Grain Fields and Degree-Day Phenology of the Cereal Leaf Beetle (Coleoptera: Chrysomelidae) in Utah: Long-Term Patterns. J. Econ. Entomol. 107 (1), 240–249. https://doi.org/10.1603/EC13387.

Fahad, S., Bajwa, A.A., Nazir, U., Anjum, S.A., Farooq, A., Zohaib, A., Sadia, S., Nasim, W., Adkins, S., Saud, S., Ihsan, M.Z., Alharby, H., Wu, C., Wang, D., Huang, J., 2017. Crop Production under Drought and Heat Stress: Plant Responses and Management Options. Front. Plant Sci. 8, 1147. https://doi.org/10.3389/fpls.2017.01147.

Fang, Y., Qiu, X., Guo, T., Wang, Y., Cheng, T., Zhu, Y., Chen, Q., Cao, W., Yao, X., Niu, Q., Hu, Y., Gui, L., 2020. An automatic method for counting wheat tiller number in the field with terrestrial LiDAR. Plant Methods 16 (1), 132. https://doi.org/10.1186/s13007-020-00672-8.

Farkas, Z., Anda, A., Vida, G., Veisz, O., Varga, B., 2021. CO2 Responses of Winter Wheat, Barley and Oat Cultivars under Optimum and Limited Irrigation. Sustainability 13 (17), 9931. https://doi.org/10.3390/su13179931.

Fowler, D.B., Gusta, L.V., Slinkard, A.E., Hobin, B., 1983. New Frontiers in Winter Wheat Production. University of Saskatchewan, Division of Extension and Community Relations.

Frederick, J.R., Camberato, J.J., 1995. Water and Nitrogen Effects on Winter Wheat in the Southeastern Coastal Plain: II. Physiological Responses. Agron. J. 87 (3), 527–533. https://doi.org/10.2134/agronj1995.00021962008700030022x.

Gaso, D.V., Berger, A.G., Ciganda, V.S., 2019. Predicting wheat grain yield and spatial variability at field scale using a simple regression or a crop model in conjunction with Landsat images. Comput. Electron. Agric. 159, 75–83. https://doi.org/10.1016/j.compag.2019.02.026.

He, Z., Joshi, A.K., Zhang, W., 2013. In: Climate Vulnerability. Elsevier, pp. 57–67.

Hokmalipour, S., Darb, M. H., Branch, A. (2011). Effects of Nitrogen Fertilizer on Chlorophyll Content and Other Leaf Indicate in Three Cultivars of Maize (Zea mays L.).

Ishikura, K., Fueki, N., Suda, T., Sugikawa, Y., Tou, S., 2020. Estimation of nitrogen uptake and tiller number of winter wheat using a handheld optical sensor in Hokkaido, Japan. Soil Science and Plant Nutrition 66 (6), 828–836. https://doi.org/10.1080/00380768.2020.1829455.

Jarasiunas, G., 2016. Assessment of the agricultural land under steep slope in Lithuania. J. Cent. Eur. Agric. 17 (1), 176–187. https://doi.org/10.5513/JCEA01/17.1.1688.

Jiang, J., Wang, C., Wang, H., Fu, Z., Cao, Q., Tian, Y., Zhu, Y., Cao, W., Liu, X., 2021. Evaluation of Three Portable Optical Sensors for Non-Destructive Diagnosis of Nitrogen Status in Winter Wheat. Sensors 21 (16), 5579. https://doi.org/10.3390/s21165579.

Khabbazan, S., Vermunt, P., Steele-Dunne, S., Ratering Arntz, L., Marinetti, C., van der Valk, D., Iannini, L., Molijn, R., Westerdijk, K., van der Sande, C., 2019. Crop Monitoring Using Sentinel-1 Data: A Case Study from The Netherlands. Remote Sens. (Basel) 11 (16), 1887. https://doi.org/10.3390/rs11161887.

Kokhan, S., Vostokov, A., 2020. Using Vegetative Indices to Quantify Agricultural Crop Characteristics. *Journal of*. Ecol. Eng. 21 (4), 120–127. https://doi.org/10.12911/22998993/119808.

Kouadio, L., Duveiller, G., Djaby, B., El Jarroudi, M., Defourny, P., Tychon, B., 2012. Estimating regional wheat yield from the shape of decreasing curves of green area index temporal profiles retrieved from MODIS data. Int. J. Appl. Earth Observat. Geoinformat. 18, 111–118. https://doi.org/10.1016/j.jag.2012.01.009.

Lancashire, P.D., Bleiholder, H., Boom, T.V.D., Langelüddeke, P., Stauss, R., Weber, E., Witzenberger, A., 1991. A uniform decimal code for growth stages of crops and weeds. Ann. Appl. Biol. 119 (3), 561–601. https://doi.org/10.1111/j.1744-7348.1991.tb04895.x.

Ledent, J.F., 1982. Morphology and Yield in Winter Wheat Grown in High Yielding Conditions. Crop Sci. 22 (6), 1115–1120. https://doi.org/10.2135/cropsci1982.0011183X002200060008x.

Li, D., Wang, X., Zheng, H., Zhou, K., Yao, X., Tian, Y., Zhu, Y., Cao, W., Cheng, T., 2018. Estimation of area- and mass-based leaf nitrogen contents of wheat and rice crops from water-removed spectra using continuous wavelet analysis. Plant Methods 14 (1), 76. https://doi.org/10.1186/s13007-018-0344-1.

Liland, K.H., Stefansson, P., Indahl, U.G., 2020. Much faster cross-validation in PLSR-modelling by avoiding redundant calculations. Journal of Chemometrics 34 (3). https://doi.org/10.1002/cem.3201.

Liu, L., Wang, J., Huang, W., Zhao, C., Zhang, B., Tong, Q., 2004. Estimating winter wheat plant water content using red edge parameters. Int. J. Remote Sens. 25 (17), 3331–3342. https://doi.org/10.1080/01431160310001654365.

Liu, Y., Qian, J., Yue, H., 2021. Comprehensive evaluation of Sentinel-2 red edge and shortwave-infrared bands to estimate soil moisture. IEEE J. Selected Topics Appl. Earth Observat. Remote Sens. 14, 7448–7465. https://doi.org/10.1109/JSTARS.2021.3098513.

Lynch, J.P., Doyle, D., McAuley, S., McHardy, F., Danneels, Q., Black, L.C., White, E.M., Spink, J., 2017. The impact of variation in grain number and individual grain weight on winter wheat yield in the high yield potential environment of Ireland. Eur. J. Agron. 87, 40–49. https://doi.org/10.1016/j.eja.2017.05.001.

Lynch, J., Spink, J., Doyle, D., Hackett, R., Phelan, S., Forristal, D., Kildea, S., Glynn, L., Plunkett, M., Wall, D., Hutton, F., Hennessy, M., 2016. The Winter Wheat Guide. Teagasc. https://www.teagasc.ie/media/website/publications/2016/Winter-Wheat-Guide.pdf.

Marshall, M., Belgiu, M., Boschetti, M., Pepe, M., Stein, A., Nelson, A., 2022. Field-level crop yield estimation with PRISMA and Sentinel-2. ISPRS J. Photogramm. Remote Sens. 187, 191–210. https://doi.org/10.1016/j.isprsjprs.2022.03.008.

Milne, B.F., Toker, Y., Rubio, A., Nielsen, S.B., 2015. Unraveling the Intrinsic Color of Chlorophyll. Angewandte Chemie 127 (7), 2198–2201. https://doi.org/10.1002/ange.201410899.

Mu, H., Jiang, D., Wollenweber, B., Dai, T., Jing, Q., Cao, W., 2010. Long-term Low Radiation Decreases Leaf Photosynthesis, Photochemical Efficiency and Grain Yield in Winter Wheat. J. Agron. Crop Sci. 196 (1), 38–47. https://doi.org/10.1111/j.1439-037X.2009.00394.x.

Mulla, D.J., 2013. Twenty five years of remote sensing in precision agriculture: Key advances and remaining knowledge gaps. Biosyst. Eng. 114 (4), 358–371. https://doi.org/10.1016/j.biosystemseng.2012.08.009.

Ouaadi, N., Jarlan, L., Ezzahar, J., Zribi, M., Khabba, S., Bouras, E., Bousbih, S., Frison, P.-L., 2020. Monitoring of wheat crops using the backscattering coefficient and the interferometric coherence derived from Sentinel-1 in semi-arid areas. Remote Sens. Environ. 251, 112050 https://doi.org/10.1016/j.rse.2020.112050.

Reich, P.B., Walters, M.B., Kloeppel, B.D., Ellsworth, D.S., 1995. Different photosynthesis-nitrogen relations in deciduous hardwood and evergreen coniferous tree species. Oecologia 104 (1), 24–30. https://doi.org/10.1007/BF00365558.

Richter, K., Hank, T.B., Vuolo, F., Mauser, W., D'Urso, G., 2012. Optimal Exploitation of the Sentinel-2 Spectral Capabilities for Crop Leaf Area Index Mapping. Remote Sens. (Basel) 4 (3), 561–582. https://doi.org/10.3390/rs4030561.

Rodríguez, D., Keltjens, W.G., Goudriaan, J., 1998. Plant leaf area expansion and assimilate production in wheat (Triticum aestivum L.) growing under low phosphorus conditions. Plant and Soil 200 (2), 227–240. https://doi.org/10.1023/A:1004310217694.

Roth, L., Camenzind, M., Aasen, H., Kronenberg, L., Barendregt, C., Camp, K.-H., Walter, A., Kirchgessner, N., Hund, A., 2020. Repeated Multiview Imaging for Estimating Seedling Tiller Counts of Wheat Genotypes Using Drones. Plant Phenomics 2020, 1–20.

Ruan, C., Dong, Y., Huang, W., Huang, L., Ye, H., Ma, H., Guo, A., Ren, Y., 2021. Prediction of Wheat Stripe Rust Occurrence with Time Series Sentinel-2 Images. Agriculture 11 (11), 1079. https://doi.org/10.3390/agriculture11111079.

Sadras, V.O., Villalobos, F.J., Fereres, E., 2016. Crop Development and Growth. In: Villalobos, F.J., Fereres, E. (Eds.), Principles of Agronomy for Sustainable Agriculture. Springer International Publishing, pp. 141–158. https://doi.org/10.1007/978-3-319-46116-8_11.

Segarra, J., Buchaillot, M.L., Araus, J.L., Kefauver, S.C., 2020. Remote Sensing for Precision Agriculture: Sentinel-2 Improved Features and Applications. Agronomy 10 (5), 641. https://doi.org/10.3390/agronomy10050641.

Serrano, L., Filella, I., Peñuelas, J., 2000. Remote Sensing of Biomass and Yield of Winter Wheat under Different Nitrogen Supplies. Crop Sci. 40 (3), 723–731. https://doi.org/10.2135/cropsci2000.403723x.

Skakun, S., Vermote, E., Roger, J.-C., Franch, B., 1 Department of Geographical Sciences, University of Maryland, College Park, MD 20742, USA, & 2 NASA Goddard Space Flight Center Code 619, 8800 Greenbelt Road, Greenbelt, MD 20771, USA. (2017). Combined Use of Landsat-8 and Sentinel-2A Images for Winter Crop Mapping and Winter Wheat Yield Assessment at Regional Scale. AIMS Geosci., 3(2), 163–186. https://doi.org/10.3934/geosci.2017.2.163.

Song, Y., Wang, J., 2019. Winter wheat canopy height extraction from UAV-based point cloud data with a moving cuboid filter. Remote Sens. (Basel) 11 (10), 1239. https://doi.org/10.3390/rs11101239.

Sylvester-Bradley, R., Berry, P., Blake, J., Kindred, D., Spink, J., Bingham, I., McVittie, J., Foulkes, J., 2018. Wheat Growth Guide. AHDB Cereals & Oilseeds. https://ahdb.org.uk/knowledge-library/wheat-growth-guide.

Tao, H., Feng, H., Xu, L., Miao, M., Yang, G., Yang, X., Fan, L., 2020. Estimation of the yield and plant height of winter wheat using UAV-based hyperspectral images. Sensors 20 (4), 1231. https://doi.org/10.3390/s20041231.

ten Harkel, J., Bartholomeus, H., Kooistra, L., 2019. Biomass and crop height estimation of different crops using UAV-based lidar. Remote Sens. (Basel) 12 (1), 17. https://doi.org/10.3390/rs12010017.

Thorp, K.R., Wang, G., West, A.L., Moran, M.S., Bronson, K.F., White, J.W., Mon, J., 2012. Estimating crop biophysical properties from remote sensing data by inverting linked radiative transfer and ecophysiological models. Remote Sens. Environ. 124, 224–233. https://doi.org/10.1016/j.rse.2012.05.013.

Wang, R., Wang, Y., Hu, Y., Dang, T., Guo, S., 2021. Divergent responses of tiller and grain yield to fertilization and fallow precipitation: Insights from a 28-year long-term experiment in a semiarid winter wheat system. J. Integr. Agric. 20 (11), 3003–3011. https://doi.org/10.1016/S2095-3119(20)63296-8.

Wu, F., Wang, J., Zhou, Y., Song, X., Ju, C., Sun, C., Liu, T., 2022. Estimation of Winter Wheat Tiller Number Based on Optimization of Gradient Vegetation Characteristics. Remote Sens. (Basel) 14 (6), 1338. https://doi.org/10.3390/rs14061338.

Wu, Y., Xu, W., Huang, H., Huang, J., Yin, F., Ma, H., Zhuo, W., Gao, X., Shen, Q., Wang, X., 2020. Winter Wheat Yield Estimation at the Field Scale By Assimilating Sentinel-2 LAI into Crop Growth Model. In: IGARSS 2020–2020 IEEE International

Geoscience and Remote Sensing Symposium, pp. 4383–4386. https://doi.org/10.1109/IGARSS39084.2020.9323941.

Xie, Q., Dash, J., Huete, A., Jiang, A., Yin, G., Ding, Y., Peng, D., Hall, C.C., Brown, L., Shi, Y., Ye, H., Dong, Y., Huang, W., 2019. Retrieval of crop biophysical parameters from Sentinel-2 remote sensing imagery. Int. J. Appl. Earth Observat. Geoinformat. 80, 187–195. https://doi.org/10.1016/j.jag.2019.04.019.

Xu, X., Wang, J., Li, C., Song, X., & Huang, W. (2010). Estimating growth height of winter wheat with remote sensing (C. M. U. Neale & A. Maltese, Eds.; p. 782428). https://doi.org/10.1117/12.864909.

Xue, Q., Weiss, A., Baenziger, P., 2004. Predicting phenological development in winter wheat. Climate Res. 25, 243–252. https://doi.org/10.3354/cr025243.

Yue, J., Feng, H., Yang, G., Li, Z., 2018. A comparison of regression techniques for estimation of above-ground winter wheat biomass using near-surface spectroscopy. Remote Sens. (Basel) 10 (2), 66. https://doi.org/10.3390/rs10010066.

Zahir, S.A.D.M., Omar, A.F., Jamlos, M.F., Azmi, M.A.M., Muncan, J., 2022. A review of visible and near-infrared (Vis-NIR) spectroscopy application in plant stress detection. Sens. Actuators, A 338, 113468. https://doi.org/10.1016/j.sna.2022.113468.

Zhang, H., Du, H., Zhang, C., Zhang, L., 2021. An automated early-season method to map winter wheat using time-series Sentinel-2 data: A case study of Shandong, China. Comput. Electron. Agric. 182, 105962 https://doi.org/10.1016/j.compag.2020.105962.